Comprehensive analysis of RNA m6A methylation in pressure overload-induced cardiac hypertrophy

Weidong Li[1], Chenxv Xing[1], Limeng Bao[1], Shengna Han[2], Tianxia Luo[3], Zhiju Wang[1] and Hongkun Fan[1*]

Abstract

Aim: To analyze and compare the mRNA N^6-methyladenosine modifications in transverse aortic constriction induced mice hearts and normal mice hearts.

Materials and methods: Colorimetric quantification was used to probe the changes in m^6A modifications in the total RNA. The expression of m^6A-related enzymes was analyzed via qRT-PCR and western blotting. RNA-seq and MeRIP-seq were performed to identify genes with differences in m^6A modifications or expression in the transcriptome profile.

Results: Compared with the control group, the TAC group exhibited higher m^6A methylation levels. FTO and WTAP were downregulated after TAC, while METTL3 was significantly downregulated at the protein level. MeRIP-seq revealed that 1179 m^6A peaks were upmethylated and 733 m^6A peaks were downmethylated, and biological analysis of these genes exhibited a strong relationship with heart function.

Conclusion: Our findings provide novel information regarding m^6A modification and gene expression changes in cardiac hypertrophy, which may be fundamental for further research.

Keywords: Cardiac hypertrophy, m^6A transcriptome, MeRIP-seq

Introduction

Cardiac hypertrophy is an adaptive response to myocardial contractility and cardiac function [1]. Cardiac tissues exhibit plasticity and can respond to changes in the external environment [2]. Cardiac hypertrophy is characterized by myocardial thickening, for reasons unclear, as well as increased myocardial cell volume, increased protein synthesis, sarcomere remodeling, and myocardial fibrosis. The continuous development of cardiac hypertrophy, induced by various mechanical stimuli and

neurohumoral factors, may eventually lead to ventricular dilation, heart failure, malignant arrhythmias, or sudden death [3, 4]. However, there has been no significant breakthrough in the research on blocking and reversal of myocardial remodeling.

The N^6-methyladenosine (m^6A) modification is a post-transcriptional modification that is widely present in all regions of the mRNA [5]. Although early studies have confirmed this modification as the most common and abundant type of mRNA modification, its function is not clear [6]. Jia et al. (2011) [7] found that the fat mass and obesity-associated (FTO) protein is related to the reversible modification of m^6A in the mRNA. Using siRNA to induce the degradation of FTO mRNA results in an increase in the amount of m^6A in the mRNA, while the construction of specific vectors to express *FTO* leads to

*Correspondence: fanhk@zzu.edu.cn

[1] Department of Physiology and Neurobiology, School of Basic Medical Sciences, Zhengzhou University, No.100 Kexuedadao Road, Zhengzhou 450000, China
Full list of author information is available at the end of the article

Li *et al. BMC Genomics*   (2022) 23:576

Page 2 of 15

decreased m⁶A levels in the cells. Subsequently, experimental data have increasingly shown that the RNA m⁶A methylation requires the participation of three types of molecules: writers, erasers, and readers [8]. Methyltransferase-like 3 (METTL3) and methyltransferase-like 14 (METTL14) are the most common writers, and are primarily responsible for the addition of methyl groups to the sixth N atom of specific nucleotide bases in the mRNA, whereas FTO and AlkB homolog 5 (ALKBH5) act as erasers for demethylation to remove m⁶A modifications [9–11]. Readers are responsible for recognizing and exerting m⁶A modifications in the mRNAs [12–14]. For example, YTH domain-containing protein 1 recognizes m⁶A modifications in the mRNA and promotes mRNA export, translation, and alternative splicing [15, 16]. Currently, studies are being conducted on the regulation of m⁶A RNA methylation in various cardiovascular diseases. However, post-transcriptional regulation of the mRNA, which can affect the expression of key proteins and cardiac function in pathological cardiac hypertrophy and heart failure, remains in the initial exploration phase.

In this study, to further explore the relationship between m⁶A modification and myocardial hypertrophy and to study the role of m⁶A modification in the development of myocardial hypertrophy in mice, we obtained the whole-transcriptome profiles of altered m⁶A modifications after hypertrophy using RNA-seq and MeRIP-seq techniques on normal and hypertrophic mice heart tissues, and investigated the biological functions of these differential m⁶A modifications and gene expressions genes. We believe that this research will be useful for further therapy in cardiac hypertrophy.

Materials and methods
Animals and tissue collection
In this study, male C57BL/6 J mice (aged six weeks) were used and randomly assigned to transverse aortic constriction (TAC) or control groups. Prior to surgery, all mice were housed under a 12 h light/dark cycle with free access to food and water for at least seven days. Four weeks after TAC was performed by ligating the aortic arch between the brachiocephalic trunk and left common carotid artery through the placement of a 27-gauge needle, mice in both groups were sacrificed under isoflurane anesthesia. Thereafter, the heart tissues of both groups were collected and stored at -80 °C until further experimentation. All experimental procedures were approved by the animal ethics committee at the University of Zhengzhou, China (SCXK-2017–0001).

Cardiac (echocardiography) function
Mice in both groups were anesthetized with 1.5% isoflurane and M-mode echocardiograms were used to detect cardiac function. Ejection fraction (EF%), fractional shortening (FS%), internal dimension at end-diastole (LVID.d) and at end-systolic (LVID.s), left ventricular posterior wall thickness at end-systolic (LVPW.s) and at end-diastole (LVPW.d), interventricular septal thickness at end-systolic (IVS.s) and at end-diastole (IVS.d) were measured.

Histology analysis
The heart weight normalized to body weight (HW/BW) and lung weight normalized to body weight (LW/BW) were measured after the mice were killed. For histopathological studies, the paraffin-embedded heart tissues were sectioned at a thickness of 5 μm. Hematoxylin & eosin (H&E) and Masson's trichrome staining were performed on histological sections obtained from the paraffin-embedded hearts. Wheat germ agglutinin (WGA) staining was used to analyze cardiac hypertrophy.

RNA preparation
Total RNA was extracted from the heart tissues of mice in both groups using TRIzol reagent (Invitrogen, Waltham, MA, USA), according to the manufacturer's instructions. The quality and quantity of the total RNA was evaluated by using NanoDrop-2000 (Thermo Fisher Scientific, Waltham, MA, USA).

Quantification of m⁶A in total RNA
Total RNA from six samples per group was used for the quantification of m⁶A modifications using the colorimetric quantification method (P-9005, EpiGentek, Farmingdale, NY, USA). Briefly, a single-point positive control was used, as recommended by the manufacturer. Total RNA (200 ng), negative control, and diluted positive control were added to 96-well plates and a binding solution was used to bind RNA to the 96-well plates. The binding solution from each well was removed after 90 min and each well was washed three times with diluted wash buffer. Next, the capture antibody, detection antibody, and enhancer solution were added to capture m⁶A RNA and each well was washed with diluted wash buffer after each step. Finally, the developer solution and stop solution were added to each well to stop the enzyme reaction. The absorbance of each well was read using a microplate reader at 450 nm, and the percentage of m⁶A in total RNA was calculated.

Quantitative real-time polymerase chain reaction (qRT-PCR)
mRNA expression levels of m⁶A-related genes *METTL3*, *WTAP*, *ALKBH5*, *FTO*, and *METTL14* were analyzed in the TAC group and sham control using qRT-PCR. In brief, total RNA was extracted from both groups as

Li *et al. BMC Genomics*   (2022) 23:576

Page 3 of 15

previously described, and cDNA was obtained via reverse transcription using the PrimeScript™ RT reagent Kit with gDNA Eraser (Perfect Real Time, TakaraBio, Japan). RT-PCR was performed using the TB Green Master Mix (Tli RNaseH Plus, TakaraBio). All procedures were performed in accordance with the manufacturer's instructions. The primer sequences used are listed in Table 1.

Western blotting

Proteins were extracted from the heart tissues using RIPA lysis buffer (Solarbio, Beijing, China) containing 1 mmol/L phenylmethylsulfonyl fluoride (Solarbio) for western blotting analysis. Briefly, approximately 50 μg protein was subjected to sodium dodecyl sulfate–polyacrylamide gel electrophoresis and transferred to a polyvinylidene membrane (Millipore, Burlington, MA, USA), which was then incubated with the primary antibodies. Then, the membranes were incubated with horseradish peroxidase (HRP)-conjugated goat anti-mouse IgG or HRP-conjugated goat anti-rabbit IgG after washing with tris-buffered saline containing 0.1% Tween 20. Glyceraldehyde 3-phosphate dehydrogenase was used as the internal control. The antibodies used in this study were METTL3 (1:2000; 15,073–1-AP, ProteinTech, Rosemont, IL, USA), ALKBH5 (1:10,000; 16,837–1-AP, ProteinTech), WTAP (1:10,000; 60,188–1-Ig, ProteinTech), FTO (1:2000; ab280081, Abcam, Cambridge, UK), BMP4 (1:1000; ab39973, Abcam, Cambridge, UK), and GAPDH (1:20,000; 60,004–1-Ig, ProteinTech).

MeRIP-seq and RNA-seq

After four weeks of transverse aortic constriction surgery, three biological replicates were performed for sham and TAC group, we randomly selected three samples from each group for sequence. The m6A-IP-Seq

Table 1 Primers used for qRT-PCR

Genes	Primer types	Primer Sequences (5'-3')
METTL3	Forward	CGCTGCCTCCGATGTTGATCTG
METTL3	Reverse	CTGACTGACCTTCTTGCTCTGCTG
METTL14	Forward	TGCAGCACCTCGGTCATTTA
METTL14	Reverse	TAACCCCACTTTCGCAAGCA
WTAP	Forward	GAAGGAGACACGACAGCAGTTGG
WTAP	Reverse	GCTTGTGACCTCTGCCTGATCTAC
FTO	Forward	ATGAAGACGCTGTGCCACTGTG
FTO	Reverse	CACGTTGTAGGCTGCTCTGCTC
ALKBH5	Forward	GCAAGGTGAAGAGCGGCATCC
ALKBH5	Reverse	GTCCACCGTGTGCTCGTTGTAC
GAPDH	Forward	GGTTGTCTCCTGCGACTTCA
GAPDH	Reverse	TGGTCCAGGGTTTCTTACTCC

and RNA-seq services were provided by CloudSeq, Inc., Shanghai, China. After four weeks of TAC, total RNA was extracted from the heart tissues of mice in both groups, and 50 μg of mouse total RNA (TAC and control) was used for MeRIP-seq. Briefly, before RNA was immunoprecipitated with the m6A antibody, total RNA was randomly fragmented to obtain the fragments of 200 nt. Protein A/G beads were used to combine the m6A antibody through rotation for 1 h at room temperature. Afterward, the RNA fragments were added to the immunocapture solution and rotated for 4 h to ensure proper mixing. The beads were then resuspended with Elution Buffer to release the RNA.

For RNA-seq, rRNAs should be removed from total RNA using NEBNext rRNA Depletion Kit (New England Biolabs, Inc., Ipswich, MA, USA). RNA libraries of m6A-IP-Seq and RNA-seq were constructed using the NEBNext® Ultra II Directional RNA Library Prep Kit (New England Biolabs Inc.), and the libraries were qualified using an Agilent 2100 BioAnalyzer system (Agilent Technologies, Inc., Santa Clara, CA, USA) and sequenced on a NovaSeq platform (Illumina, Inc., San Diego, CA, USA).

Briefly, raw data were obtained after quality controlled with Q30. Cutadapt software v1.9.3 was used to remove low-quality reads, and Hisat2 software v2.0.4 was used to align the clean reads to the reference genome [17]. To identify m6A methylated regions on the mRNA and differentially methylated sites between the two groups, MACS and diffReps software were used [18, 19]. Altered m6A peaks with fold change > 2 and *p*-value undergo false discovery rate < 0.01 (*p*-value cutoff of < 0.0001 were default selection criteria of diffReps software, then undergo false discovery rate correction) were selected for gene ontology and pathway enrichment analyses [20–23].

The differentially methylated and expression genes were divided into two groups (upregulation or downregulation) and subjected to gene ontology analysis and pathway enrichment analysis. The background gene list used in this analysis were detected genes in RNA-seq, and genes with an average of less than 10 reads per sample were omitted. The gene ontology analysis was performed using (www.geneontology.org, current release 2022–03) and pathway enrichment analysis was performed using clusterProfiler R package (v4.2), the *p*-value denotes the significance of GO term enrichment of the genes, the Fisher *p*-value denotes the significance of the pathway correlated to the conditions. Then all *p*-value undergo FDR (Benjamini & Hochberg) correction.

MeRIP-qPCR

In this experiment, EpiQuik™ CUT&RUN m6A RNA Enrichment (MeRIP) Kit (P-9018, EpiGentek, Farmingdale, NY, USA) was used to enrich an RNA fragment

Li *et al. BMC Genomics* (2022) 23:576

Page 4 of 15

containing m⁶A. After 4/8 weeks of TAC, the heart tissues were collected and stored at -80 °C. Total RNA was obtained as previously described, an optimal input RNA amount is 10 ug per reaction. All procedures were performed in accordance with the manufacturer's instructions. Briefly, adding m6A antibody, affinity beads and immuno capture buffer to PCR tubes. After rotate the tubes for 90 min, add nuclear digestion enhancer and cleavage enzyme mix reagents for cleavage under targets. Proteinase K and RNA binding beads were used for RNA purification. At last, resuspend the beads in 13 ul of elution buffer and transfer 13ul to a new PCR tube. The enriched RNA was used for qRT-PCR. The primer sequences used are listed in Table 2.

Statistical analyses

Data are expressed as the means ± standard deviation (SD). The unpaired Student's *t*-test was used to determine statistical significance for experiments with two groups, and a *p*-value < 0.05 was considered statistically significant (*$p < 0.05$, **$p < 0.01$).

Results

Cardiac hypertrophy in mice four weeks post TAC

M-mode echocardiograms were used to detect the ventricular structure and function of the mice in both groups (Fig. 1A). Compared with the sham group, HW/BW and LW/BW were significantly higher in the TAC group (Fig. 1B and C). Furthermore, compared with the sham group, the LVPW.d, LVPW.s, and LVID.d were significantly higher in the TAC group after four weeks; while the LVID.s, IVS.d, and IVS.s showed an increasing trend in the TAC group, but did not increase significantly (Fig. 1D–I). The ejection fraction reflects the ventricular ejection function; the left ventricular fractional shortening is an important indicator for evaluating cardiac contractility. Four weeks post TAC, the ejection function and cardiac contractility of mice in the TAC group were significantly lower than those of mice in the sham group (Fig. 1J–K).

To further verify whether the mice developed cardiac hypertrophy at four weeks post TAC, H&E, Masson's

Table 2 Primers used for MeRIP-qPCR

Genes	Primer types	Primer Sequences (5'-3')
KCNN2	Forward	CGCGTTTATTTTTGGCGCA
KCNN2	Reverse	GGAGAGCACTGGTGGACG
BMP4-1	Forward	CCCACTGAACTGAGTGCCAT
BMP4-1	Reverse	CATCCACACCCCTCTACCAC
BMP4-2	Forward	GCCGGGGCCATACCTTGA
BMP4-2	Reverse	GGCGACGGCAGTTCTTATTC

trichrome, and WGA staining were performed on histological sections generated from paraffin-embedded mice hearts. The results showed that the cardiomyocyte morphology of mice in the TAC group was altered. Compared to the sham group, the cardiomyocytes of mice in the TAC group appeared hypertrophied (Fig. 2A and B). Myocardial fibrosis in the TAC mice was simultaneously aggravated and the collagen deposition area increased at four weeks post TAC (Fig. 2C).

m⁶A methylation profiles in normal and hypertrophic mice hearts

First, we quantified m⁶A levels in the heart tissues after TAC. The results showed that m⁶A modification of total RNA was significantly higher when the mice myocardium developed hypertrophy (Fig. 3A). Based on qRT-PCR analysis, the mRNA relative expressions of five major m⁶A related enzymes, including *METTLL3, METTL14, WTAP, FTO* and *ALKBH5*, were compared between the sham and TAC groups. Four weeks post TAC, the mRNA levels of *METTL14* and *WTAP*, key methyltransferases responsible for m⁶A modifications, and the major demethyltransferase *FTO* were significantly lower in the TAC group compared with those of the sham group. Further, *METTL3* and *ALKBH5* were not significantly dysregulated (compared with the sham group) (Fig. 3B). To further investigate the reasons for the m⁶A modification changes in total RNA after TAC, we assessed the protein expression levels of *METTL3, WTAP, FTO*, and *ALKBH5* in the heart tissues. *FTO, WTAP* and *METTL3* downregulation were verified using western blotting; while the expression of demethyltransferase *ALKBH5* was upregulated, but not significantly (Fig. 3C–D).
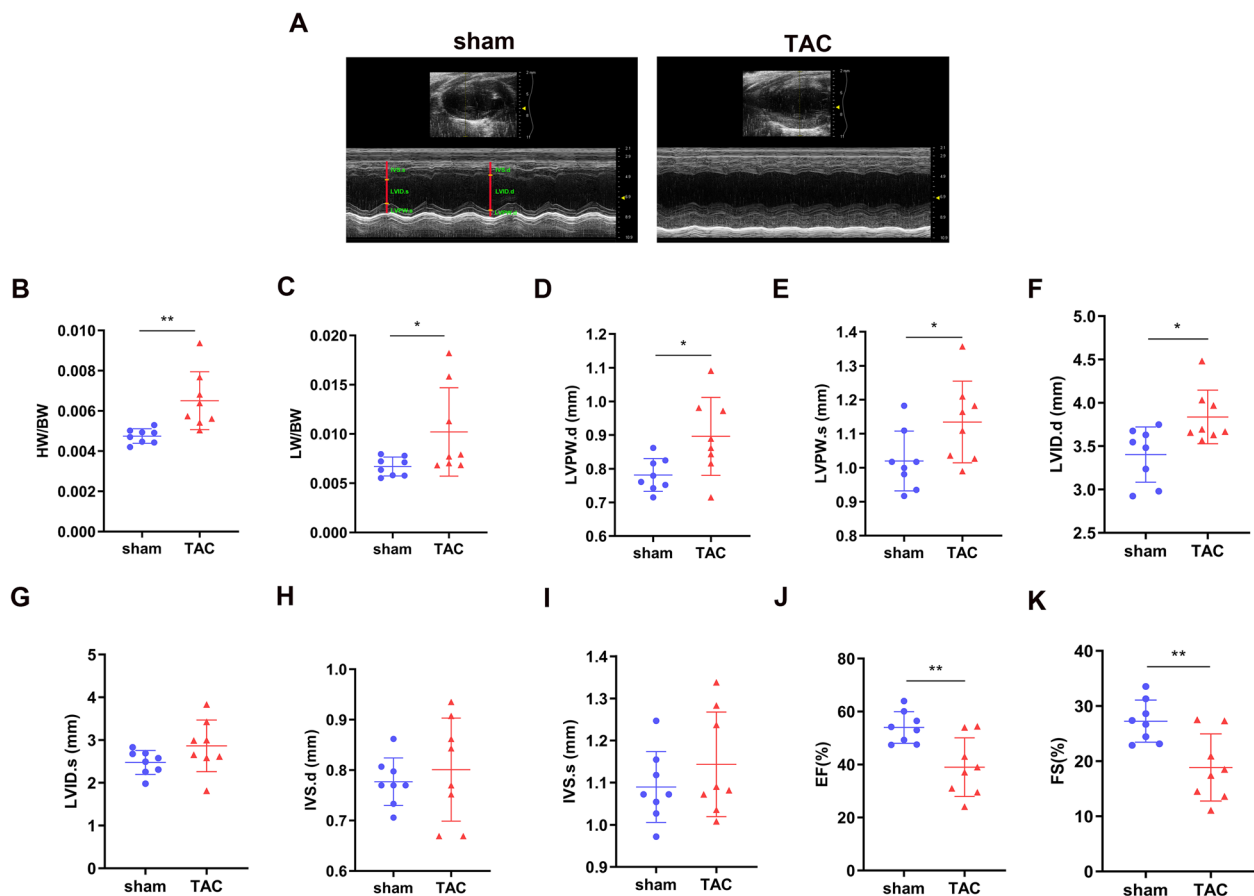
MeRIP-seq analysis of mRNA derived from mice hearts revealed 16,214 m⁶A peaks in the control group and 21,179 m⁶A peaks in the TAC group. Of these, 13,060 peaks overlapped between the control and TAC groups (Fig. 4A). All methylated N⁶-methyladenosine genes were divided into several groups according to the number of peaks per gene. Notably, most of the m⁶A-methylated coding genes in both groups contained only one or two m⁶A sites (Fig. 4B). Moreover, the number of genes in each group clearly showed that the m⁶A modification peaks in the TAC group were significantly higher than those in the sham group, which proves that the m⁶A modification level increased after TAC.

Compared with the sham group, 1179 significantly hypermethylated m⁶A peaks and 733 significantly hypomethylated m⁶A peaks were identified in the TAC group (fold change > 2 and *p*-value < 0.01). The top ten upregulated and downregulated m⁶A peaks are listed in Table 3. To analyze the distribution profiles of the m⁶A peaks within mRNAs, the peaks were categorized into five

Li *et al. BMC Genomics*   (2022) 23:576

Page 5 of 15

Fig. 1 Ventricular hypertrophy and reduced cardiac function were observed in mice after four weeks of transverse aortic constriction. **A** Representative image of mouse hearts in both groups; **B–C** Gravimetric analysis of heart weight normalized to body weight (HW/BW) and lung weight normalized to body weight (LW/BW) in both groups ($n = 8$ each); **D–I** Measurements of left ventricular posterior wall thickness at end-diastole (LVPW.d), left ventricular posterior wall thickness at end-systolic (LVPW.s), internal dimension at end-diastole (LVID.d), internal dimension at end-systolic (LVID.s), interventricular septal thickness at end-diastole (IVS.d), and interventricular septal thickness at end-systolic (IVS.s) in both groups ($n = 8$ each), respectively; **J–K** Echocardiographic ejection fraction (EF) and fractional shortening (FS) measurements in both groups ($n = 8$ each). The results are expressed as the means $\pm$ SD (*$p < 0.05$, **$p < 0.01$, compared to the Sham group)

transcript segments: 5'UTR, start codon segment, coding sequence (CDS), stop codon segment, and 3'UTR [24]. Our results showed that the m^{6}A sites were typically harbored in the CDS and stop codon segments (Fig. 4C–D). Furthermore, the distribution profiles of differentially methylated m^{6}A peaks and relative density of differentially methylated m^{6}A sites (DMMSs) in the chromosomes revealed that the dysregulated m^{6}A peaks were transcribed from all chromosomes, but genes located on chr7 and chr11 most likely underwent m^{6}A methylation changes (Fig. 4E and F). In this study, the first rank of m^{6}A motifs were characterized "AGGAAGA" in both groups (Fig. 4G). To investigate the preferential location of m^{6}A modifications in different regions of the mRNA, metagene profiles were used to visualize the differences between the two groups. The results showed that the

main differences between the two groups were concentrated in the CDS region (Fig. 4H). A representation of the significantly upmethylated and downmethylated peaks is shown in Fig. 5.

Gene Ontology (GO) and Kyoto Encyclopedia of Genes and Genomes (KEGG) pathway analyses of differentially methylated mRNA

To explore the functions of m^{6}A modifications in hypertrophic mice hearts, differentially methylated m^{6}A peaks were selected for GO and KEGG pathway analysis. GO analysis revealed that the upregulated peaks in the hypertrophic heart tissues were significantly associated with the system development and anatomical structure development (Fig. 6A), cellular anatomical entity and extracellular matrix (Fig. 6B), and protein binding and binding (Fig. 6C). The downmethylated peaks were significantly

Li *et al. BMC Genomics*   (2022) 23:576

Page 6 of 15
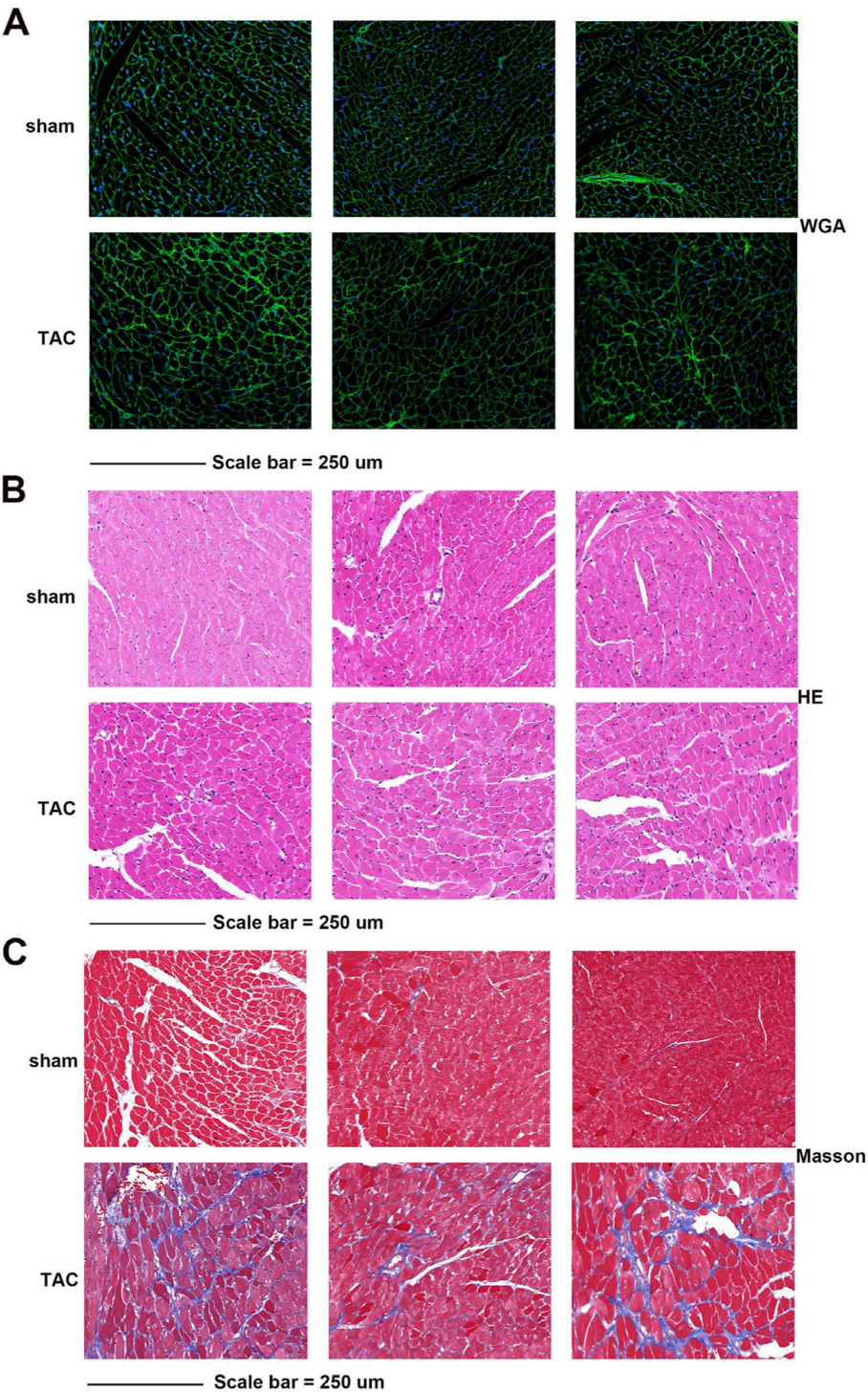
Fig. 2 Cardiac remodeling occurred after transverse aortic constriction. **A** Representative wheat germ agglutinin-stained cardiac cross-sections from the transverse aortic constriction (TAC) and control groups. **B** Representative hematoxylin and eosin-stained cardiac cross-sections from TAC and control groups; **C** Representative results of Masson's trichrome staining to assess fibrosis of mice heart tissues; Scale bar = 250 μm

Li *et al. BMC Genomics*   (2022) 23:576

Page 7 of 15

Fig. 3 Changes in m[6]A levels after transverse aortic constriction were caused by increased methyltransferase or decreased demethyltransferases. **A** Increased m.[6]A in RNA in mice hypertrophic hearts; **B** qRT-PCR was performed to analyze mRNA levels of *METTL3*, *ALKBH5*, *WTAP*, *METTL14*, and *FTO* in both groups (*n* = 6 each); **C** Representative immunoblots; **D** Densitometry quantification of protein (*n* = 3 ~ 5 each). The results are expressed as the means ± SD (**p* < 0.05, compared to the sham group)

associated with heart processes and heart contraction (Fig. 6D), intracellular and cellular anatomical entity (Fig. 6E), and binding and protein binding (Fig. 6F).

Pathway analysis showed that the upmethylated peaks in hypertrophic heart tissues were significantly associated with focal adhesion and extracellular matrix-receptor interaction (Fig. 6G). The downmethylated peaks were significantly associated with hypertrophic cardiomyopathy and diabetic cardiomyopathy (Fig. 6H).

Analysis of RNA-binding proteins (RBPs) of differentially methylated mRNAs

To exert the biological function of m[6]A modifications, RBPs that recognize specific sites are necessary. In this study, the RMBase v2.0 database was used to identify potential RBPs of differentially methylated m[6]A sites.

Relative information about m[6]A modification sites and the support list of RBPs was obtained from this database. In total, we identified 20 potential RBPs in the upmethylated peaks and 19 (missing Jarid2) potential RBPs in the downmethylated peaks. The RBPs were highly distributed in the differentially methylated m[6]A sites with a fold change (log2) of approximately 2. According to the percentage of RBP-bound m[6]A sites in the differentially methylated m[6]A sites, this distribution is presented as a heatmap in Fig. 7, which shows that Cstf2, Ago2, and Mbnl3 are widely distributed.

Conjoint analysis of m[6]A-RIP-seq and RNA-seq data

RNA-seq was used to obtain the data of differentially expressed genes in hypertrophic mice hearts. Compared with the control group, 1281 significantly higher genes

Li *et al. BMC Genomics*   (2022) 23:576

Page 8 of 15
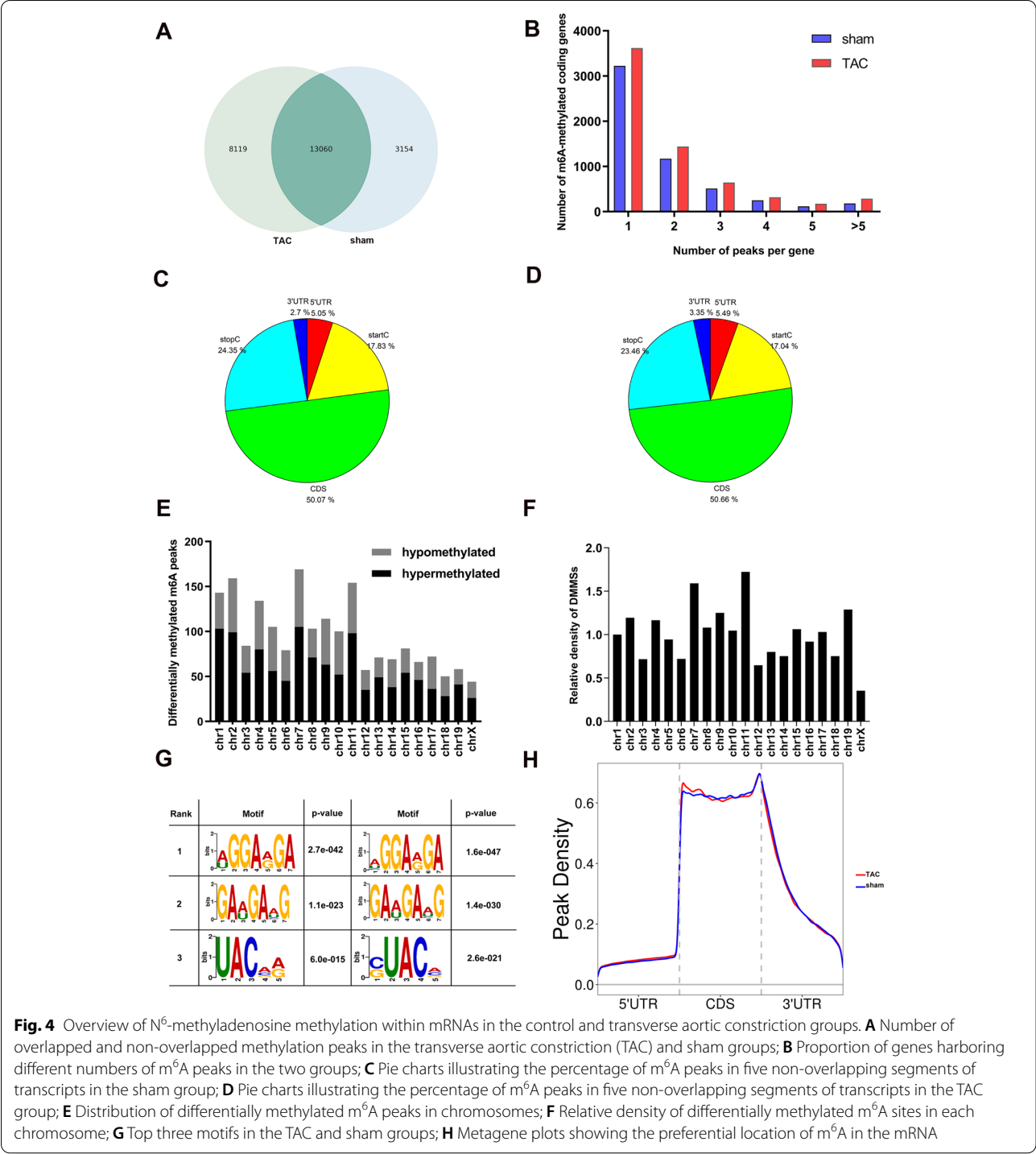
Fig. 4 Overview of N[6]-methyladenosine methylation within mRNAs in the control and transverse aortic constriction groups. **A** Number of overlapped and non-overlapped methylation peaks in the transverse aortic constriction (TAC) and sham groups; **B** Proportion of genes harboring different numbers of m[6]A peaks in the two groups; **C** Pie charts illustrating the percentage of m[6]A peaks in five non-overlapping segments of transcripts in the sham group; **D** Pie charts illustrating the percentage of m[6]A peaks in five non-overlapping segments of transcripts in the TAC group; **E** Distribution of differentially methylated m[6]A peaks in chromosomes; **F** Relative density of differentially methylated m[6]A sites in each chromosome; **G** Top three motifs in the TAC and sham groups; **H** Metagene plots showing the preferential location of m[6]A in the mRNA

and 154 significantly lower genes (fold change > 2 and $p < 0.05$) were identified in the TAC group (Fig. 8A). Hierarchical clustering was performed to identify distinguishable gene expression patterns between TAC and sham group (Fig. 8B). Based on the conjoint analysis of RNA-seq and MeRIP-seq data, we found that the upmethylated

protein-coding genes were more likely to have higher transcription expression (70.6% with Log2FC (gene expression) > 1) and the downmethylated protein-coding genes were more likely to have lower transcription expression (13.8% with Log2FC (gene expression) < -1) (Fig. 8C-E). The effect of m[6]A modification on genes is

Li *et al. BMC Genomics*   (2022) 23:576

Page 9 of 15

Table 3 The top 20 differently methylated m6A peaks

| Chromsome	txStart	txEnd	Peak length	Gene	Fold change	*P*-value	Regulation
chr11	40,707,564	40,707,717	153	Hmmr	285.9	4.6929E-09	up
chr7	80,309,392	80,309,488	96	Prc1	203.4	5.21894E-09	up
chr2	152,912,121	152,912,360	239	Mylk2	162	3.60657E-09	up
chr19	38,060,080	38,060,200	120	Cep55	160.9	3.73133E-09	up
chr9	85,844,141	85,844,580	439	Tpbg	154.2	7.1048E-13	up
chr11	78,304,045	78,304,280	235	Spag5	146.4	1.05539E-11	up
chr19	37,420,301	37,420,620	319	Kif11	145.2	2.68469E-09	up
chr3	8,993,740	8,993,820	80	Tpd52	142.9	1.91831E-11	up
chr1	134,327,257	134,327,360	103	Ppfia4	128.3	6.51387E-09	up
chr10	93,464,061	93,464,185	124	Lta4h	127.3	7.89094E-09	up
chr2	54,084,401	54,085,060	659	Rprm	186.3	1.1801E-09	down
chr17	13,227,021	13,227,097	76	Smok2a	152.1	2.92825E-09	down
chr4	143,370,101	143,370,440	339	Lrrc38	138.8	3.4094E-09	down
chr17	46,304,156	46,304,460	304	Abcc10	132.9	1.0497E-09	down
chr14	47,292,061	47,292,280	219	Socs4	132.6	3.22531E-10	down
chr10	104,185,961	104,185,992	31	Gm20765	132.4	1.26028E-09	down
chr5	114,612,781	114,612,980	199	Fam222a	123	1.41896E-11	down
chr10	122,449,061	122,449,460	399	Avpr1a	116.1	2.46993E-11	down
chr14	110,754,701	110,754,980	279	Slitrk6	114.9	3.24827E-09	down
chr15	76,715,301	76,715,580	279	Lrrc24	114.6	3.95801E-09	down
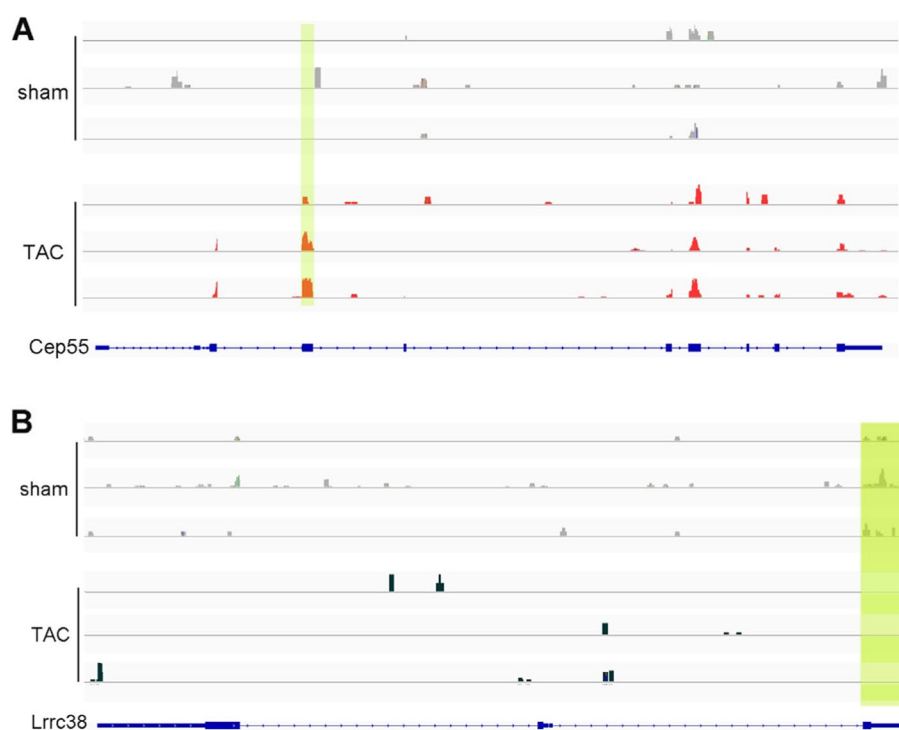
Fig. 5 Differentially methylated m6A peaks in the sham and transverse aortic constriction groups. **A** Hypermethylated gene visualized in the Integrative Genomics Viewer; **B** Hypomethylated gene visualized in the Integrative Genomics Viewer
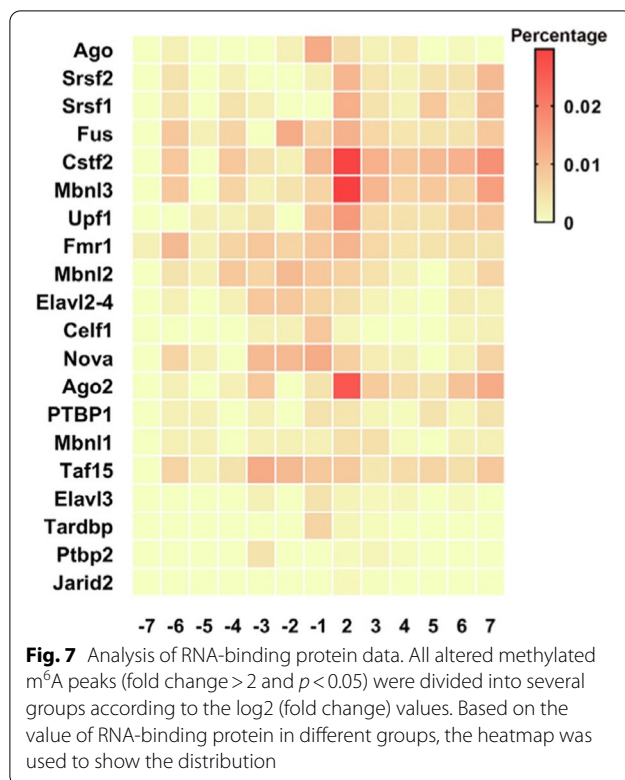
Li *et al. BMC Genomics*   (2022) 23:576

Page 10 of 15
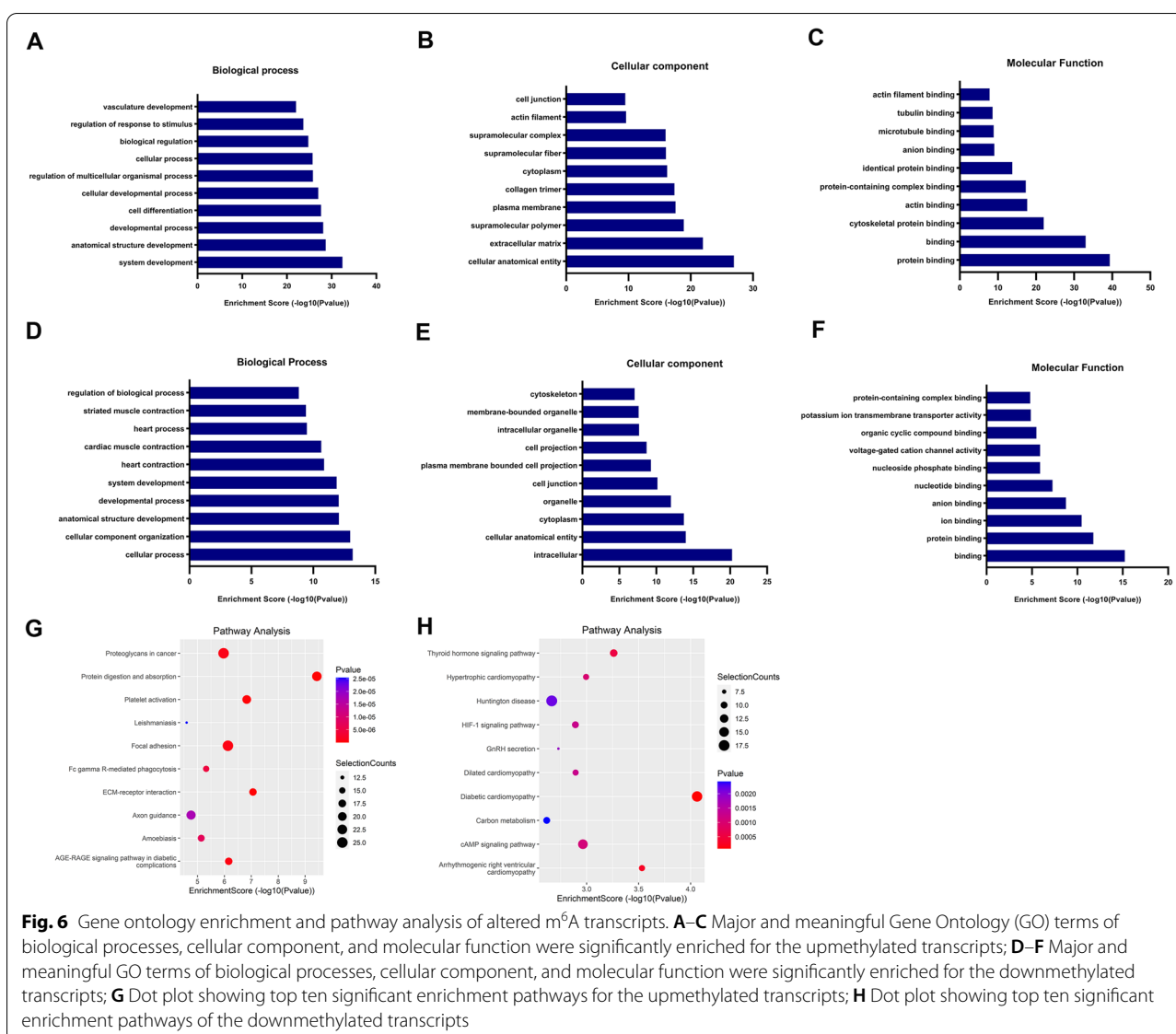
Fig. 6 Gene ontology enrichment and pathway analysis of altered m^{6}A transcripts. **A–C** Major and meaningful Gene Ontology (GO) terms of biological processes, cellular component, and molecular function were significantly enriched for the upmethylated transcripts; **D–F** Major and meaningful GO terms of biological processes, cellular component, and molecular function were significantly enriched for the downmethylated transcripts; **G** Dot plot showing top ten significant enrichment pathways for the upmethylated transcripts; **H** Dot plot showing top ten significant enrichment pathways of the downmethylated transcripts

mainly achieved by m^{6}A reader proteins, which suggests that when cardiac hypertrophy occurs, changes in the level of m^{6}A modification on mRNA are likely to affect the binding of stability-related reader proteins.

M^{6}A modification enhancing KCNN2 and BMP4 mRNA stability in cardiac hypertrophy

KCNN2 is a voltage-independent K$^+$ channel activated by intracellular Ca^{2+}, expressed in almost all excitable cells, and BMP4 is a member of the bone morphogenetic protein family [25, 26]. Both KCNN2 and BMP4 have been confirmed to play essential roles in cardiac hypertrophy. The abnormal expression of KCNN2 after cardiac hypertrophy may be related to some important heart process [27]. BMP4 act as a pro-hypertrophic factor in

the heart. Many studies have shown that BMP4 is related to the development of the heart and mediated cardiomyocyte hypertrophy and myocardial fibrosis [28, 29]. To verify the effect of m^{6}A methylation modification on gene expression, we detected m^{6}A modification level and mRNA expression level of KCNN2 and BMP4 after TAC (relevant information was obtained from MeRIP-seq and RNA-seq). Based on MeRIP-qPCR and qRT-PCR analysis, the m^{6}A modification level and mRNA expression level of KCNN2 were significantly decreased compared with the control group after four weeks of TAC (Fig. 9A and B). Moreover, there are two methylated m^{6}A sites on BMP4 mRNA which were significantly increased compared with the control group (Fig. 9C and D), and the

Li *et al. BMC Genomics*   (2022) 23:576

Page 11 of 15

Fig. 7 Analysis of RNA-binding protein data. All altered methylated m⁶A peaks (fold change > 2 and *p* < 0.05) were divided into several groups according to the log2 (fold change) values. Based on the value of RNA-binding protein in different groups, the heatmap was used to show the distribution

mRNA expression level of BMP4 was also significantly increased compared with the control group (Fig. 9E).

Notably, the immunoblots results showed that the precursor and mature of BMP4 protein were significantly increased at four weeks post-TAC, but markedly decreased at eight weeks post-TAC (Fig. 9F and G). So we further detected the m⁶A modification level and mRNA expression level of BMP4 at eight weeks post-TAC to verify that the changes in protein expression level were caused by m⁶A modification. The results of M-mode echocardiograms showed that after eight weeks of TAC, HW/BW, LW/BW and left ventricular posterior wall thickness were significantly increased in TAC group, and the mice developed myocardial hypertrophy (Fig. 9H-K). Subsequently, we found that the upregulated of the two methylated m⁶A sites on BMP4 mRNA measured at four weeks post-TAC disappeared (Fig. 9L and M), and the mRNA expression levels of BMP4 was not significantly changed compared with the control group (Fig. 9N). Besides, the KCNN2 and BMP4 mRNA expression levels

in this study were consistent with the results of RNA-seq (GSE182985) obtained from GEO database. Taken together, these results indicate that m⁶A modification may promotes KCNN2 and BMP4 mRNA stability when mice develop cardiac hypertrophy.
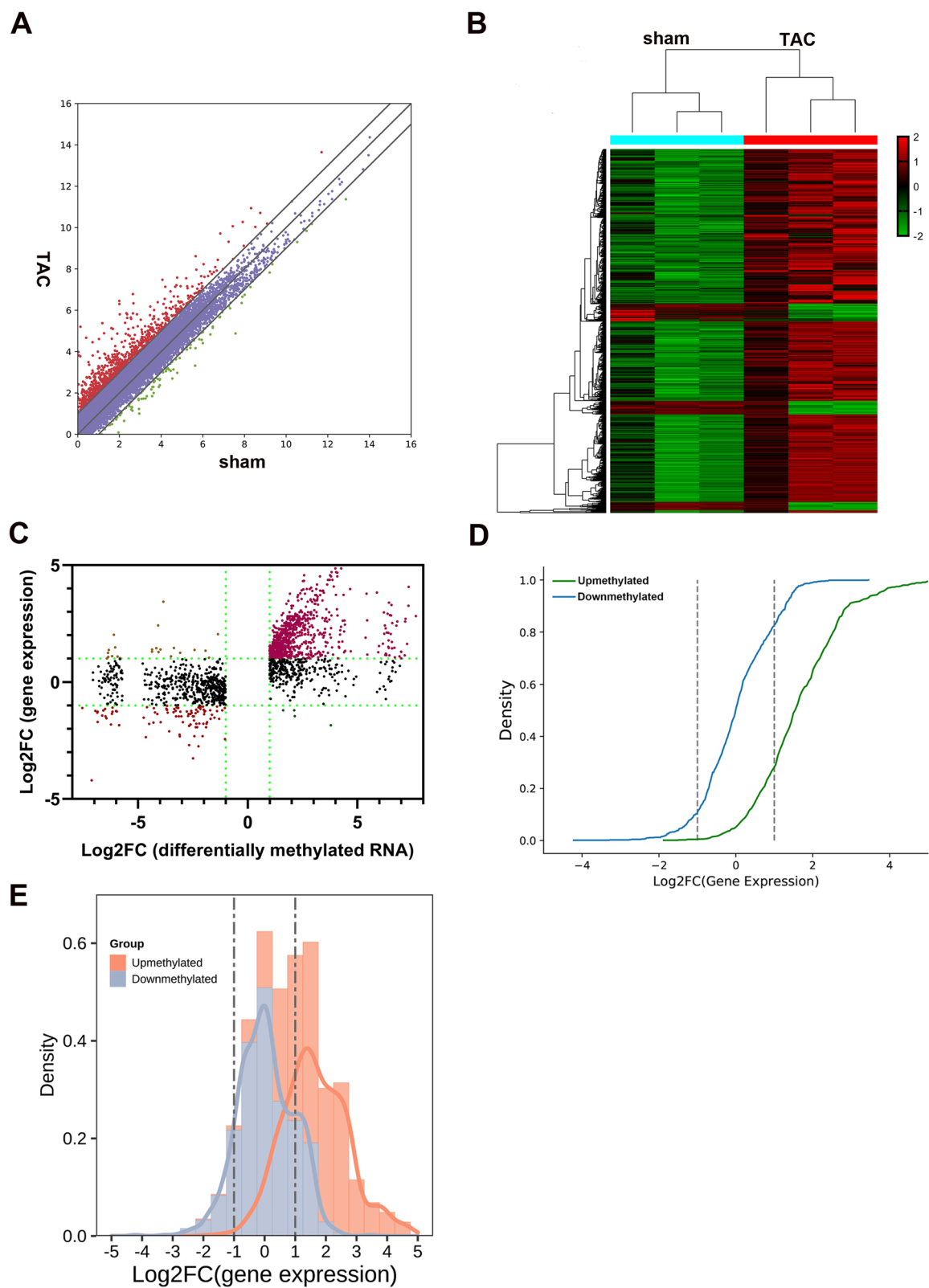
Discussion

In this study, TAC was performed to cause pressure overload in mice hearts to induce cardiac hypertrophy. We observed that the cardiac tissue responds to changes in the environment, such as increased cardiomyocyte volume in the face of mechanical overload, to compensate for variation in cardiac function, thereby maintaining normal cardiac function despite hypertrophy. Studies have confirmed that m⁶A modifications in the body also respond to changes in the environment and time. For example, when neonatal cardiomyocytes develop until the seventh day, the m⁶A modification level decreases, which may be related to the downregulation of *METTL3* expression [30]. Additionally, altered m⁶A modifications may affect the proliferative capacity of cardiomyocytes [31].

This study found that cardiac hypertrophy occurred in mice four weeks post TAC and the level of m⁶A modification of total RNA increased in hypertrophic heart tissues, which may be related to changes in the expression of these key methyltransferases or demethylases. The results of qRT-PCR and western blotting analyses showed that the gene and protein expressions of *FTO* and *WTAP* were significantly downregulated, whereas the mRNA level of *METTL3* showed no significant change, but there was an increase in the protein expression. However, it is unclear whether the altered level of m⁶A modification after hypertrophy is mediated by a single enzyme or by the synergy of multiple enzymes; this requires further studying. However, the key methyltransferase *METTL3* may play an important role in cardiac hypertrophy, and studies have found that *METTL3* may be a key regulatory factor in increasing m⁶A methylation levels after hypertrophy. The inhibition of *METTL3* in mice hearts can lead to heart failure, whereas the overexpression of *METTL3* promotes the development of hypertrophy in cardiomyocytes, highlighting the critical importance of m⁶A RNA methylation in the heart for maintaining normal cardiac function [32]. In addition, we focused on the profiles of altered m⁶A modified transcripts and gene
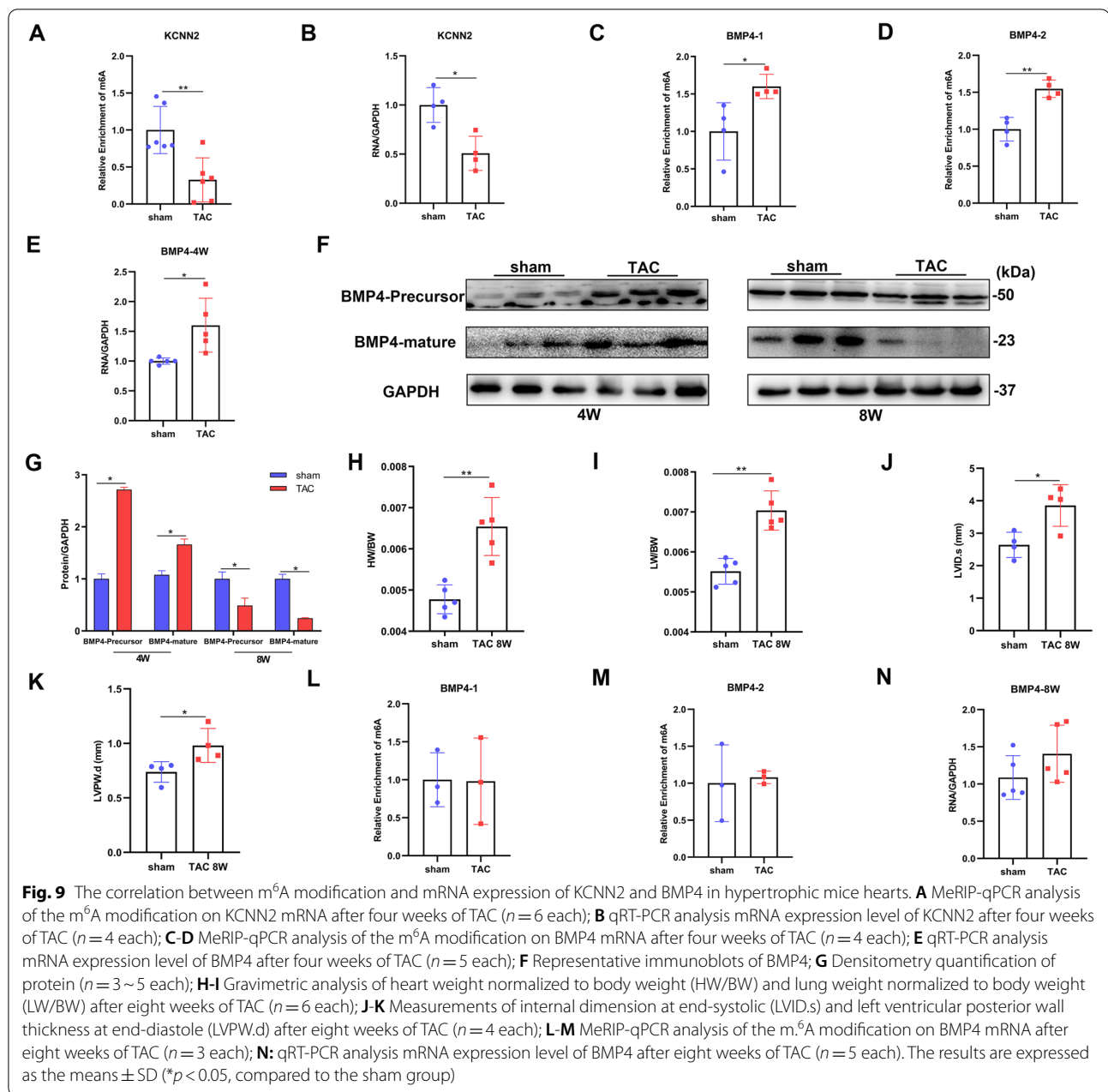
(See figure on next page.)
Fig. 8 Conjoint analysis of MeRIP-seq and RNA-seq data from hypertrophic heart tissues in mice. **A** Differentially expressed mRNAs between sham and transverse aortic constriction groups (TAC) (fold changes > 2 and *p* < 0.05); **B** Distribution pattern of altered genes; **C** Distribution of transcripts with a significant change in both m⁶A level and expression after TAC, genes with Log2 fold change > 1 were divided by using green dashed lines; **D** Cumulative distribution function plot showing the correlation between the genes with differentially methylated and expression; **E** Histogram and probability density function plot showing the distribution of two groups base on gene expression

Li *et al. BMC Genomics*   (2022) 23:576

Page 12 of 15

Fig. 8 (See legend on previous page.)

Fig. 9 The correlation between m⁶A modification and mRNA expression of KCNN2 and BMP4 in hypertrophic mice hearts. **A** MeRIP-qPCR analysis of the m⁶A modification on KCNN2 mRNA after four weeks of TAC ($n=6$ each); **B** qRT-PCR analysis mRNA expression level of KCNN2 after four weeks of TAC ($n=4$ each); **C**-**D** MeRIP-qPCR analysis of the m⁶A modification on BMP4 mRNA after four weeks of TAC ($n=4$ each); **E** qRT-PCR analysis mRNA expression level of BMP4 after four weeks of TAC ($n=5$ each); **F** Representative immunoblots of BMP4; **G** Densitometry quantification of protein ($n=3\sim5$ each); **H-I** Gravimetric analysis of heart weight normalized to body weight (HW/BW) and lung weight normalized to body weight (LW/BW) after eight weeks of TAC ($n=6$ each); **J**-**K** Measurements of internal dimension at end-systolic (LVID.s) and left ventricular posterior wall thickness at end-diastole (LVPW.d) after eight weeks of TAC ($n=4$ each); **L**-**M** MeRIP-qPCR analysis of the m.⁶A modification on BMP4 mRNA after eight weeks of TAC ($n=3$ each); **N:** qRT-PCR analysis mRNA expression level of BMP4 after eight weeks of TAC ($n=5$ each). The results are expressed as the means $\pm$ SD (*$p<0.05$, compared to the sham group)

expression after hypertrophy, and biological function analysis of these changed genes was performed.

Analysis of the distribution profiles of m⁶A peaks within mRNAs in heart tissues revealed that the m⁶A sites are typically harbored in CDS and stop codon segments [33]. Furthermore, the results of the preferential location of m⁶A modifications showed that the main differences between the two groups were concentrated in the CDS region. This was also confirmed by IGV alignment of genes with differential m⁶A modifications in the MeRIP-seq data, suggesting that the effect of m⁶A

modifications on cardiac hypertrophy may be related to its effects, such as altering translation and mRNA splicing, on the CDS region of the mRNA [34, 35].

GO and KEGG pathway analyses of differentially methylated genes showed a strong correlation with heart function, such as heart process and heart contraction (ontology: biological process), hypertrophic cardiomyopathy, and dilated cardiomyopathy (pathway analysis). We also used the RMBase v2.0 database to identify potential RBPs of differentially methylated m⁶A sites, and the results showed that Cstf2, Ago2, and Mbnl3

Li *et al. BMC Genomics* (2022) 23:576

Page 14 of 15

were widely distributed, which may play a critical role in RNA splicing through RNA binding [36].

Finally, based on a conjoint analysis of MeRIP-seq and RNA-seq data, we found that the higher the methylation ratio, the higher the transcription expression, which was consistent with studies in patients with high myopia [37]. In this study, we found the m[6]A modification level of BMP4 and KCNN2 were consistent with their gene expression. This suggests that changes in the level of m[6]A modification of genes are likely to affect gene expression [38]. At present, many studies have confirmed that YT521-B homology (YTH) and insulin-like growth factor 2 mRNA-binding protein (IGF2BP) domain play a role in mRNA stabilization, translation and degradation by recognizing methylated m[6]A sites on genes [39–41]. The conjoint analysis of MeRIP-seq and RNA-seq data in this study suggest that when the level of m[6]A modification increases, the expression of the gene may increase by promoting the stability of the gene. One of the features of cardiac hypertrophy is increased protein synthesis, which suggests that m[6]A modification may play an important role in cardiac hypertrophy through increases the expression of related proteins genes by stabilizes target mRNA [42]. Furthermore, previous studies have shown m[6]A modification promoted YTHDF2 protein expression through enhancing Ythdf2 mRNA stability in cardiac hypertrophy [43]. In addition, many genes with changes in both m[6]A modification and gene expression are related to cardiac processes, such as *Myh7*, *bmp4* and *Ttn*, which were shown to be related to hypertrophic cardiomyopathy [44–47]. These results may provide guidance for future studies on the role of m[6]A methylation in cardiac hypertrophy.

Conclusion

In conclusion, we performed m[6]A-RIP-seq and RNA-seq to analyze the transcriptome profiles of genes with altered m[6]A modification and expression, revealing the potential functions of altered transcripts and RBPs, thereby providing a fundamental contribution to future studies on cardiac hypertrophy.

Supplementary Information

The online version contains supplementary material available at https://doi.org/10.1186/s12864-022-08833-w.

Additional file 1: Supplemental figure 1. Full length of representative immunoblots.

Authors' contribution
W Li and H Fan conceived the project and designed the protocol; W Li, C Xing, L Bao, S Han, T Luo and Z Wang performed the experiments; W Li and H Fan performed the data analysis; W Li and H Fan wrote the manuscript. The author(s) read and approved the final manuscript.

Availability of data and materials
The authors confirm that the data supporting the findings of this study are available within the article. The m[6]A-sequencing and RNA-sequencing datasets have been submitted to the GEO database under the accession number GSE201764.

Declarations

Ethics approval and consent to participate
All methods were carried out in accordance with relevant guidelines and regulations of Zhengzhou University. All animals were handled in accordance with the Animal Research: Reporting of in vivo Experiments (ARRIVE) guidelines and the University of Zhengzhou Institutional Animal Care and Use Committee policies. All experimental procedures were approved by the animal ethics committee at the University of Zhengzhou, China (SCXK-2017–0001).

Consent for publication
Not applicable.

Competing interests
The authors declare that they have no competing interest.

Author details
[1]Department of Physiology and Neurobiology, School of Basic Medical Sciences, Zhengzhou University, No.100 Kexuedadao Road, Zhengzhou 450000, China. [2]Department of Pharmacology, School of Basic Medical Sciences, Zhengzhou University, No.100 Kexuedadao Road, Zhengzhou 450000, China. [3]Department of Physiology, School of Medicine, Henan University of Chinese Medicine, No.156 Jinshui Road, Zhengzhou 450052, China.

References
1. Shimizu I, Minamino T. Physiological and pathological cardiac hypertrophy. J Mol Cell Cardiol. 2016;97:245–62.
2. van Berlo JH, Maillet M, Molkentin JD. Signaling effectors underlying pathologic growth and remodeling of the heart. J Clin Invest. 2013;123(1):37–45.
3. Heineke J, Molkentin JD. Regulation of cardiac hypertrophy by intracellular signalling pathways. Nat Rev Mol Cell Biol. 2006;7(8):589–600.
4. Perrino C, Naga Prasad SV, Mao L, Noma T, Yan Z, Kim HS, Smithies O, Rockman HA. Intermittent pressure overload triggers hypertrophy-independent cardiac dysfunction and vascular rarefaction. J Clin Invest. 2006;116(6):1547–60.
5. Meyer KD, Patil DP, Zhou J, Zinoviev A, Skabkin MA, Elemento O, Pestova TV, Qian SB, Jaffrey SR. 5′UTR m(6)A Promotes Cap-Independent Translation. Cell. 2015;163(4):999–1010.
6. Wei CM, Gershowitz A, Moss B. Methylated nucleotides block 5′terminus of HeLa cell messenger RNA. Cell. 1975;4(4):379–86.
7. Jia G, Fu Y, Zhao X, Dai Q, Zheng G, Yang Y, Yi C, Lindahl T, Pan T, Yang YG, et al. N6-methyladenosine in nuclear RNA is a major substrate of the obesity-associated FTO. Nat Chem Biol. 2011;7(12):885–7.
8. Meyer KD, Jaffrey SR. Rethinking m(6)A Readers, Writers, and Erasers. Annu Rev Cell Dev Biol. 2017;33:319–42.
9. Liu J, Yue Y, Han D, Wang X, Fu Y, Zhang L, Jia G, Yu M, Lu Z, Deng X, et al. A METTL3-METTL14 complex mediates mammalian nuclear RNA N6-adenosine methylation. Nat Chem Biol. 2014;10(2):93–5.
10. Zheng G, Dahl JA, Niu Y, Fedorcsak P, Huang CM, Li CJ, Vagbo CB, Shi Y, Wang WL, Song SH, et al. ALKBH5 is a mammalian RNA demethylase that impacts RNA metabolism and mouse fertility. Mol Cell. 2013;49(1):18–29.

Li *et al. BMC Genomics*   (2022) 23:576

Page 15 of 15

11. Ping XL, Sun BF, Wang L, Xiao W, Yang X, Wang WJ, Adhikari S, Shi Y, Lv Y, Chen YS, et al. Mammalian WTAP is a regulatory subunit of the RNA N6-methyladenosine methyltransferase. Cell Res. 2014;24(2):177–89.

12. Wang H, Zuo H, Liu J, Wen F, Gao Y, Zhu X, Liu B, Xiao F, Wang W, Huang G, et al. Loss of YTHDF2-mediated m(6)A-dependent mRNA clearance facilitates hematopoietic stem cell regeneration. Cell Res. 2018;28(10):1035–8.

13. Qin Y, Li L, Luo E, Hou J, Yan G, Wang D, Qiao Y, Tang C. Role of m6A RNA methylation in cardiovascular disease (Review). Int J Mol Med. 2020;46(6):1958–72.

14. Alarcon CR, Goodarzi H, Lee H, Liu X, Tavazoie S, Tavazoie SF. HNRNPA2B1 Is a Mediator of m(6)A-Dependent Nuclear RNA Processing Events. Cell. 2015;162(6):1299–308.

15. Liao S, Sun H, Xu C. YTH Domain: A Family of N(6)-methyladenosine (m(6)A) Readers. Genomics Proteomics Bioinformatics. 2018;16(2):99–107.

16. Wang X, Zhao BS, Roundtree IA, Lu Z, Han D, Ma H, Weng X, Chen K, Shi H, He C. N(6)-methyladenosine Modulates Messenger RNA Translation Efficiency. Cell. 2015;161(6):1388–99.

17. Kim D, Langmead B, Salzberg SL. HISAT: a fast spliced aligner with low memory requirements. Nat Methods. 2015;12(4):357–60.

18. Zhang Y, Liu T, Meyer CA, Eeckhoute J, Johnson DS, Bernstein BE, Nusbaum C, Myers RM, Brown M, Li W, et al. Model-based analysis of ChIP-Seq (MACS). Genome Biol. 2008;9(9):R137.

19. Shen L, Shao NY, Liu X, Maze I, Feng J, Nestler EJ. diffReps: detecting differential chromatin modification sites from ChIP-seq data with biological replicates. PLoS ONE. 2013;8(6):e65598.

20. Bailey TL. DREME: motif discovery in transcription factor ChIP-seq data. Bioinformatics. 2011;27(12):1653–9.

21. da Huang W, Sherman BT, Lempicki RA. Bioinformatics enrichment tools: paths toward the comprehensive functional analysis of large gene lists. Nucleic Acids Res. 2009;37(1):1–13.

22. Trapnell C, Williams BA, Pertea G, Mortazavi A, Kwan G, van Baren MJ, Salzberg SL, Wold BJ, Pachter L. Transcript assembly and quantification by RNA-Seq reveals unannotated transcripts and isoform switching during cell differentiation. Nat Biotechnol. 2010;28(5):511–5.

23. Tian L, Greenberg SA, Kong SW, Altschuler J, Kohane IS, Park PJ. Discovering statistically significant pathways in expression profiling studies. Proc Natl Acad Sci U S A. 2005;102(38):13544–9.

24. Csepany T, Lin A, Baldick CJ Jr, Beemon K. Sequence specificity of mRNA N6-adenosine methyltransferase. J Biol Chem. 1990;265(33):20117–22.

25. Luo T, Li L, Peng Y, Xie R, Yan N, Fan N, Zhang Q. The MORN domain of Junctophilin2 regulates functional interactions with small-conductance Ca(2+)-activated potassium channel subtype2 (SK2). BioFactors. 2021;47(1):69–79.

26. Hanna A, Frangogiannis NG. The Role of the TGF-beta Superfamily in Myocardial Infarction. Front Cardiovasc Med. 2019;6:140.

27. Segura AM, Frazier OH, Buja LM. Fibrosis and heart failure. Heart Fail Rev. 2014;19(2):173–85.

28. Sun B, Huo R, Sheng Y, Li Y, Xie X, Chen C, Liu HB, Li N, Li CB, Guo WT, et al. Bone morphogenetic protein-4 mediates cardiac hypertrophy, apoptosis, and fibrosis in experimentally pathological cardiac hypertrophy. Hypertension. 2013;61(2):352–60.

29. Guo WT, Dong DL. Bone morphogenetic protein-4: a novel therapeutic target for pathological cardiac hypertrophy/heart failure. Heart Fail Rev. 2014;19(6):781–8.

30. Yang C, Zhao K, Zhang J, Wu X, Sun W, Kong X, Shi J. Comprehensive Analysis of the Transcriptome-Wide m6A Methylome of Heart via MeRIP After Birth: Day 0 vs. Day 7. Front Cardiovasc Med. 2021;8:633631.

31. Mathiyalagan P, Adamiak M, Mayourian J, Sassi Y, Liang Y, Agarwal N, Jha D, Zhang S, Kohlbrenner E, Chepurko E, et al. FTO-Dependent N(6)-Methyladenosine Regulates Cardiac Function During Remodeling and Repair. Circulation. 2019;139(4):518–32.

32. Dorn LE, Lasman L, Chen J, Xu X, Hund TJ, Medvedovic M, Hanna JH, van Berlo JH, Accornero F. The N(6)-Methyladenosine mRNA Methylase METTL3 Controls Cardiac Homeostasis and Hypertrophy. Circulation. 2019;139(4):533–45.

33. Meyer KD, Saletore Y, Zumbo P, Elemento O, Mason CE, Jaffrey SR. Comprehensive analysis of mRNA methylation reveals enrichment in 3′ UTRs and near stop codons. Cell. 2012;149(7):1635–46.

34. Zhao X, Yang Y, Sun BF, Shi Y, Yang X, Xiao W, Hao YJ, Ping XL, Chen YS, Wang WJ, et al. FTO-dependent demethylation of N6-methyladenosine regulates mRNA splicing and is required for adipogenesis. Cell Res. 2014;24(12):1403–19.

35. Thorvaldsdottir H, Robinson JT, Mesirov JP. Integrative Genomics Viewer (IGV): high-performance genomics data visualization and exploration. Brief Bioinform. 2013;14(2):178–92.

36. Kmietczyk V, Riechert E, Kalinski L, Boileau E, Malovrh E, Malone B, Gorska A, Hofmann C, Varma E, Jurgensen L, et al. m6A-mRNA methylation regulates cardiac gene expression and cellular growth. Life Sci Alliance. 2019;2(2):e201800233.

37. Dominissini D, Moshitch-Moshkovitz S, Schwartz S, Salmon-Divon M, Ungar L, Osenberg S, Cesarkas K, Jacob-Hirsch J, Amariglio N, Kupiec M, et al. Topology of the human and mouse m6A RNA methylomes revealed by m6A-seq. Nature. 2012;485(7397):201–6.

38. Wen K, Zhang Y, Li Y, Wang Q, Sun J. Comprehensive analysis of transcriptome-wide m6A methylome in the anterior capsule of the lens of high myopia patients. Epigenetics. 2021;16(9):955–68.

39. Zhao Y, Shi Y, Shen H, Xie W. m(6)A-binding proteins: the emerging crucial performers in epigenetics. J Hematol Oncol. 2020;13(1):35.

40. Shi H, Wang X, Lu Z, Zhao BS, Ma H, Hsu PJ, Liu C, He C. YTHDF3 facilitates translation and decay of N(6)-methyladenosine-modified RNA. Cell Res. 2017;27(3):315–28.

41. Huang H, Weng H, Sun W, Qin X, Shi H, Wu H, Zhao BS, Mesquita A, Liu C, Yuan CL, et al. Recognition of RNA N(6)-methyladenosine by IGF2BP proteins enhances mRNA stability and translation. Nat Cell Biol. 2018;20(3):285–95.

42. Maier T, Guell M, Serrano L. Correlation of mRNA and protein in complex biological samples. FEBS Lett. 2009;583(24):3966–73.

43. Xu H, Wang Z, Chen M, Zhao W, Tao T, Ma L, Ni Y, Li W. YTHDF2 alleviates cardiac hypertrophy via regulating Myh7 mRNA decoy. Cell Biosci. 2021;11(1):132.

44. Dias GM, Lamounier Junior A, Seifert M, Barajas-Martinez H, Barr D, Sternick EB, Medina-Acosta E. Campos de Carvalho AC, Cruz Filho FES: MYH7 p.Glu903Gln Is a Pathogenic Variant Associated With Hypertrophic Cardiomyopathy. Circ Genom Precis Med. 2021;14(5):e003476.

45. Holler V, Seebacher H, Zach D, Schwegel N, Ablasser K, Kolesnik E, Gollmer J, Waltl G, Rainer PP, Verheyen S, et al. Myocardial Deformation Analysis in MYBPC3 and MYH7 Related Sarcomeric Hypertrophic Cardiomyopathy-The Graz Hypertrophic Cardiomyopathy Registry. Genes (Basel). 2021;12(10):1469.

46. Li X, Wei W, Li X, Qi L, Lu S, Wei H, Liu Y, Dong J, Zhang C, Lin T. A heterozygous TTN (c. 79,684C>T) mutant human induced pluripotent stem cell line (ZZUNEUi023-A) generated from a Kazakh patient with dilated cardiomyopathy. Stem Cell Res. 2021;57:102614.

47. Patel PN, Ito K, Willcox JAL, Haghighi A, Jang MY, Gorham JM, DePalma SR, Lam L, McDonough B, Johnson R, et al. Contribution of Noncanonical Splice Variants to TTN Truncating Variant Cardiomyopathy. Circ Genom Precis Med. 2021;14(5):e003389.

Publisher's Note